Supplementary Information for

Laser-nanoprinting-enabled multilevel nanoscale phase encoding on quartz for integrated optical diffractive devices

Haitao Luan[1,2]*, Youtao Xing[1,2], Yuchi Bai[1,2], Yibo Dong[1,2]*, Min Gu[1,2]*

[1]School of Artificial Intelligence Science and Technology, University of Shanghai for Science and Technology, Shanghai, 200093, China

[2]Institute of Photonic Chips, University of Shanghai for Science and Technology, Shanghai, 200093, China

*E-mail: haitaoluan@usst.edu.cn; dyb@usst.edu.cn; gumin@usst.edu.cn

Supplementary Note 1: Principle of amplitude encoding of handwritten digit images using an SLM.

This principle can be described using the Jones matrix formalism. As shown in Fig. S14a, the optical path for amplitude modulation consists of a polarizer, a quarter-wave plate (QWP), and a reflective SLM. The propagation process is illustrated in Fig. S14b. The fast axis of the QWP is set at 45° relative to the x-axis. Upon reflection from the SLM, this angle becomes 135° from the perspective of reflected light, and the polarizer is oriented perpendicular to the x-axis.

When light first passes through the polarizer, its Jones vector is:

$$\begin{bmatrix}0\\1\end{bmatrix} \tag{1}$$

After transmission through the QWP, the transformation is:

$$\begin{bmatrix}\frac{1}{2}+\frac{\mathrm{i}}{2} & \frac{1}{2}-\frac{\mathrm{i}}{2}\\ \frac{1}{2}-\frac{\mathrm{i}}{2} & \frac{1}{2}+\frac{\mathrm{i}}{2}\end{bmatrix}\begin{bmatrix}0\\1\end{bmatrix} \tag{2}$$

The reflective SLM can be represented as follows, where φ denotes the phase modulation introduced by the SLM.

$$\begin{bmatrix}\exp(\mathrm{i}\varphi) & 0\\ 0 & -1\end{bmatrix} \tag{3}$$

After reflection and a second pass through the QWP, we obtain:

$$\begin{aligned}&\begin{bmatrix}\frac{1}{2}+\frac{\mathrm{i}}{2} & \frac{\mathrm{i}}{2}-\frac{1}{2}\\ \frac{\mathrm{i}}{2}-\frac{1}{2} & \frac{1}{2}+\frac{\mathrm{i}}{2}\end{bmatrix}\begin{bmatrix}\exp(\mathrm{i}\varphi) & 0\\ 0 & -1\end{bmatrix}\begin{bmatrix}\frac{1}{2}+\frac{\mathrm{i}}{2} & \frac{1}{2}-\frac{\mathrm{i}}{2}\\ \frac{1}{2}-\frac{\mathrm{i}}{2} & \frac{1}{2}+\frac{\mathrm{i}}{2}\end{bmatrix}\begin{bmatrix}0\\1\end{bmatrix}\\ &=\begin{bmatrix}(1+\cos(\varphi))+\mathrm{i}*\sin(\varphi)\\ -\sin(\varphi)-\mathrm{i}*(1-\cos(\varphi))\end{bmatrix}\end{aligned} \tag{4}$$

Define the polarization angle of the light relative to the x-axis as θ. Then:

$$\tan\theta=\frac{-\sin(\varphi)-\mathrm{i}*(1-\cos(\varphi))}{(1+\cos(\varphi))+\mathrm{i}*\sin(\varphi)}=-\frac{\sin(\varphi)}{1+\cos(\varphi)}=-\tan\left(\frac{\varphi}{2}\right) \tag{5}$$

Hence,

$$\theta=-\frac{\varphi}{2} \tag{6}$$

Equation (6) shows that the polarization direction of the reflected light is directly

controlled by the SLM phase modulation. Specifically, in our experiment, when displaying handwritten digit images, the SLM phase is set to π for the digital regions and 0 elsewhere. After the light passes through the quarter-wave plate (QWP), the polarization in the digital regions becomes $-\pi/2$ (aligned with the polarizer), while it remains 0 (perpendicular to the polarizer) in the background. Consequently, after the light finally passes through the polarizer, the intensity in the handwritten digital regions remains unchanged, whereas the intensity in other regions becomes zero, thereby achieving amplitude modulation.

From the above derivation, it can be seen that amplitude modulation under this principle does not introduce phase terms.

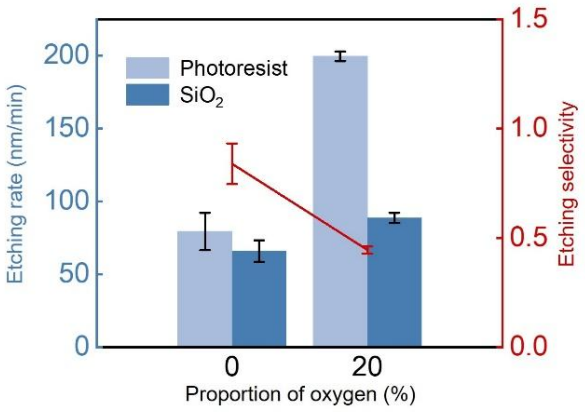

Fig. S1. Etching rate and selectivity of quartz substrate and photoresist as a function of oxygen component.

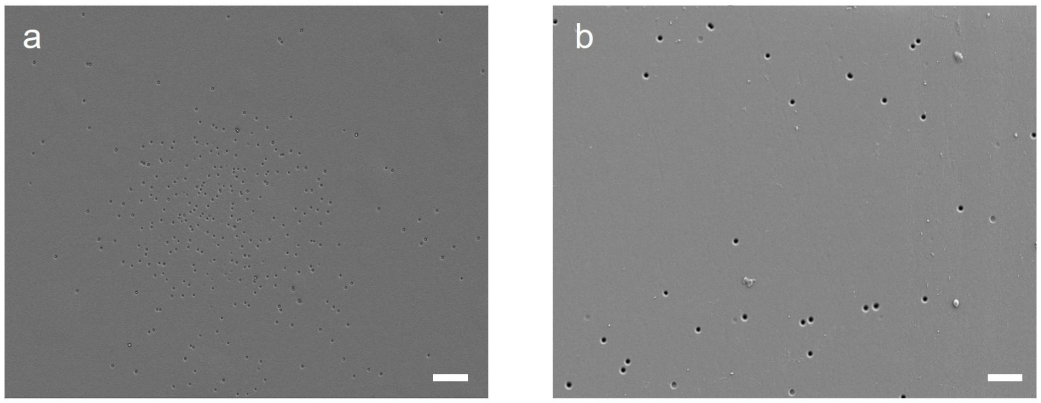

Fig. S2. SEM images of the surface morphology of the substrates after etching using different RF powers. a, 60 W. **b,** 100 W. Scale bars: 2 μm.

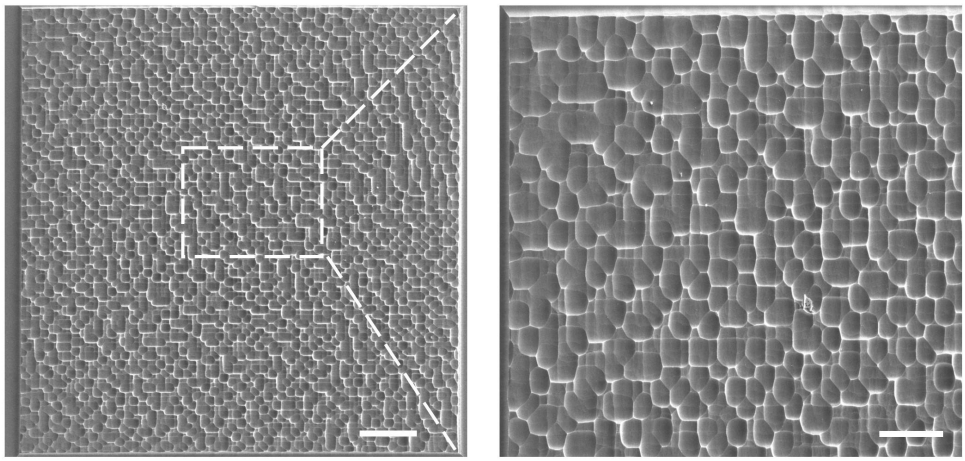

Fig. S3. SEM images of the surface morphology of the substrate after etching at a chamber pressure of 5 mTorr. Scale bars: 10 μm (left), 5 μm (right).

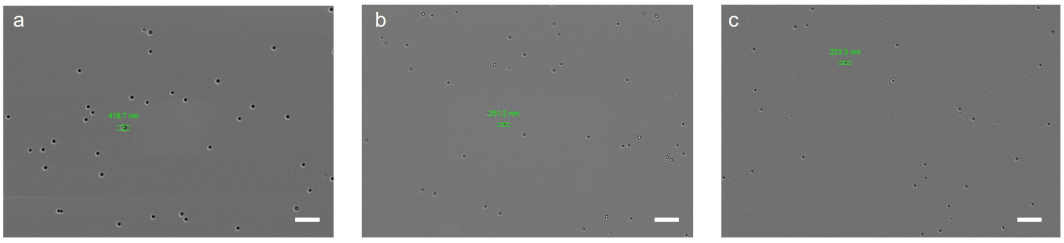

Fig. S4. SEM images of surface morphology of the substrates after etching at different chamber pressures. a, 10 mTorr. **b,** 15 mTorr. **c,** 20 mTorr. Scale bars: 2 μm.

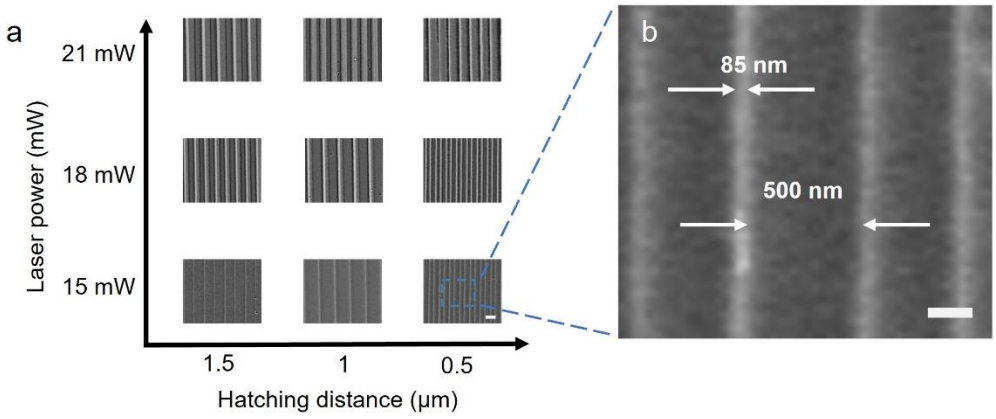

Fig. S5. SEM images of quartz samples etched using different photoresist grating masks. The masks were fabricated with varying laser powers and hatching distances. Scale bars, 1 μm and 200 nm.

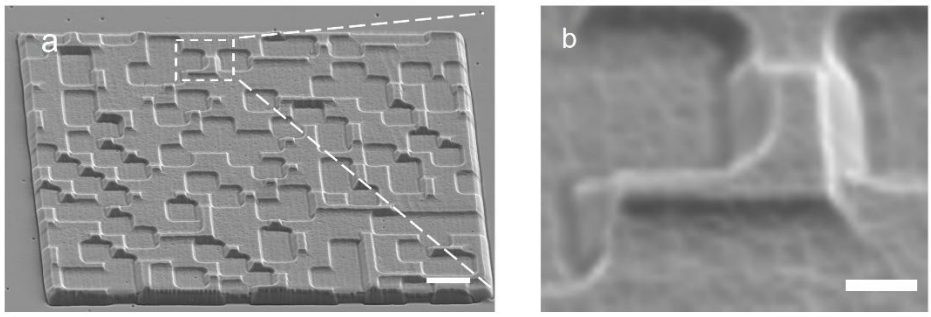

Fig. S6. Tilted SEM images of the obtained phase mask on quartz substrate. Scale bars, 4 μm and 1 μm.

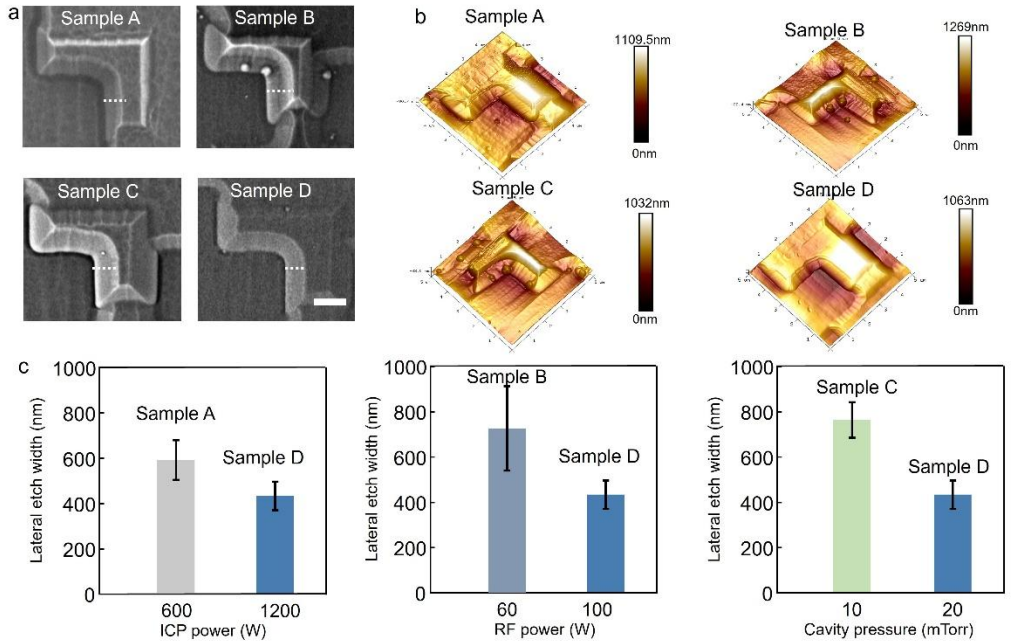

Fig. S7. Characterization of lateral etching before and after etching condition optimization. Samples A, B, and C were fabricated before optimizing ICP power, RF power, and chamber pressure, respectively, while Sample D was fabricated after applying all optimized conditions. The etching depth of all samples was kept consistent (~1 μm). a, SEM images of the samples. Scale bar, 1 μm. b, AFM images of the samples. c, Statistical comparison of lateral etching degree. Here, the lateral etching is defined as the lateral broadening at the pixel edge in the SEM images, indicated by the white dotted line in panel a. Except for the specific parameters under comparison, all other etching conditions were kept identical among samples.

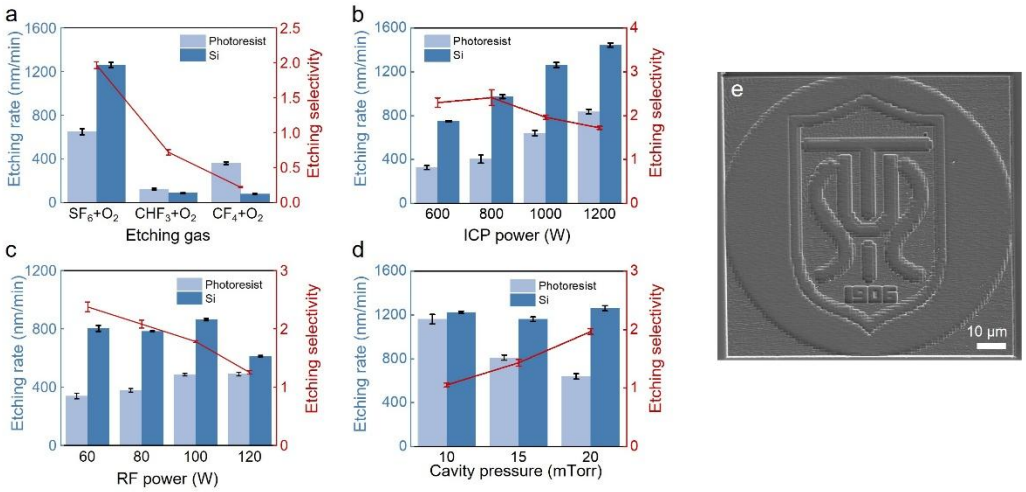

Fig. S8. Multi-parameter optimization of etching conditions for high-precision grayscale pattern transfer on Si wafers. Based on etching rate and error bar analysis, the optimized recipe was selected as SF_6/O_2 = 40/10 sccm, ICP power = 1000 W, RF power = 100 W, and chamber pressure = 20 mTorr, achieving a silicon-to-photoresist selectivity of ~1.97. a–d, Etching rate and selectivity of silicon to photoresist under different process parameters, including gas composition, ICP power, RF power, and chamber pressure. e, Demonstration of grayscale patterning on silicon, showing the etched logo of our university.

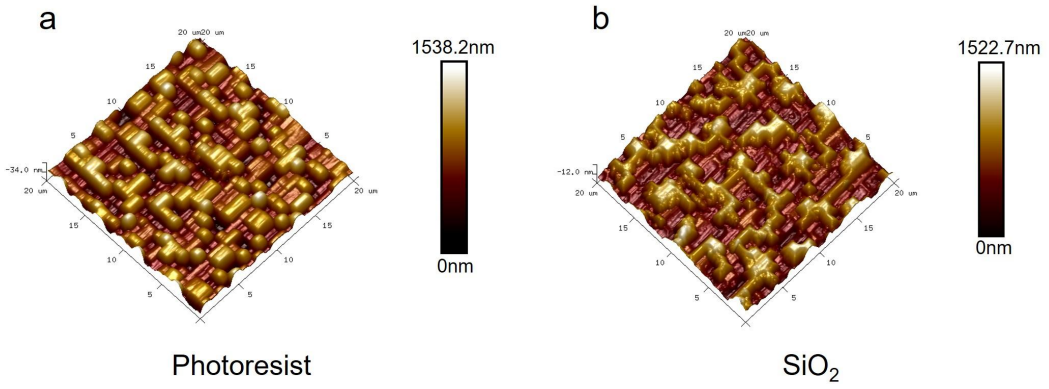

Fig. S9. Three-dimensional topography of the two holograms measured by atomic force microscopy (AFM). a The photoresist-based hologram. **b** The quartz-based hologram.

The rounded pixel edges observed mainly arise from two factors. First, the most important factor is that the photoresist mask itself exhibits rounded edges prior to etching. This originates from the two-photon polymerization mechanism in laser nano-printing, where the effective exposure volume is confined to the focal region of the objective, resulting in an ellipsoidal solidified structure with naturally rounded edges. Consequently, when the grayscale pattern is transferred onto quartz, the etched features inherit this rounded morphology. Second, the lateral isotropic etching further contributes to the smoothing of pixel boundaries. Because the mask-induced rounding is inherent to the process, it cannot be completely eliminated and causes deviations in pixel phase modulation from the ideal. However, increasing the pixel size can reduce this effect. Further improvements are also possible by employing advanced techniques to enhance the resolution of the photoresist mask.

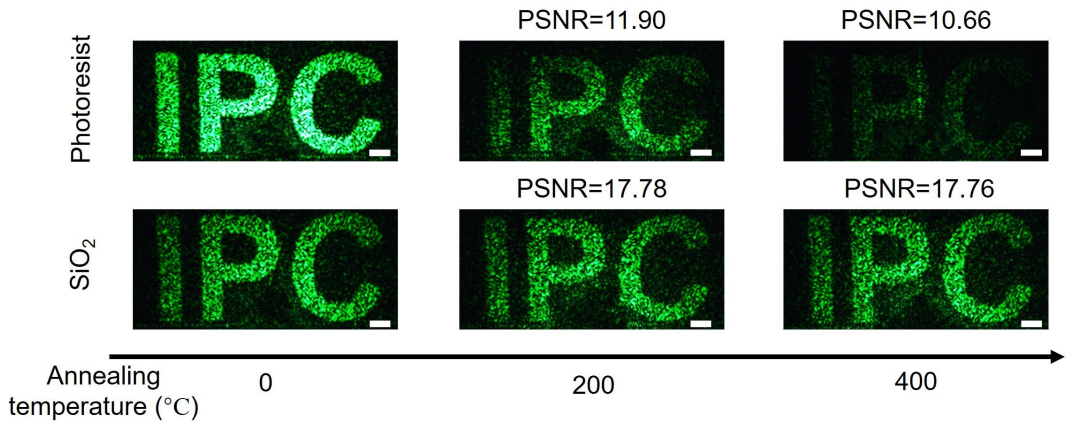

Fig. S10. Peak signal-to-noise ratios (PSNR) calculated between the original holographic image and the holographic images after annealing at different temperatures. Scale bar: 1 mm.

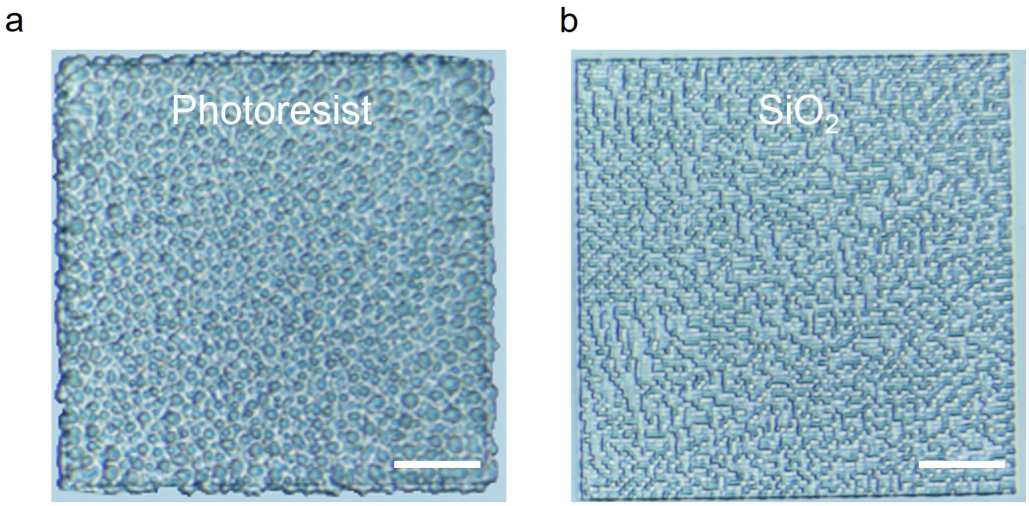

Fig. S11. Optical images of the two holograms after immersion in 25% dilute sulfuric acid for 1 min. a The photoresist-based hologram. **b** The quartz-based hologram. Scale bars: 20 μm.

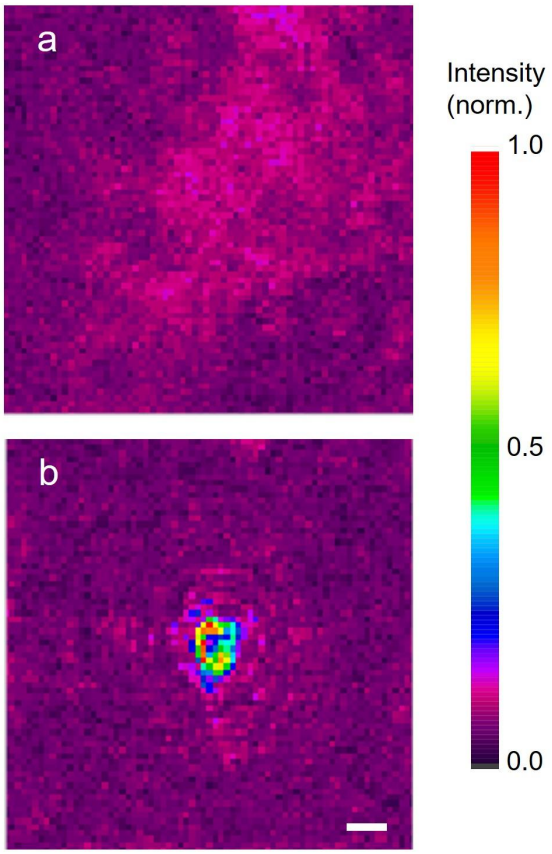

Fig. S12. Intensity distribution captured by a beam profiler. **a.** Input light field before the diffractive lens. **b.** Focused light field at the focal plane of the diffractive lens. Scale bar: 10 μm.

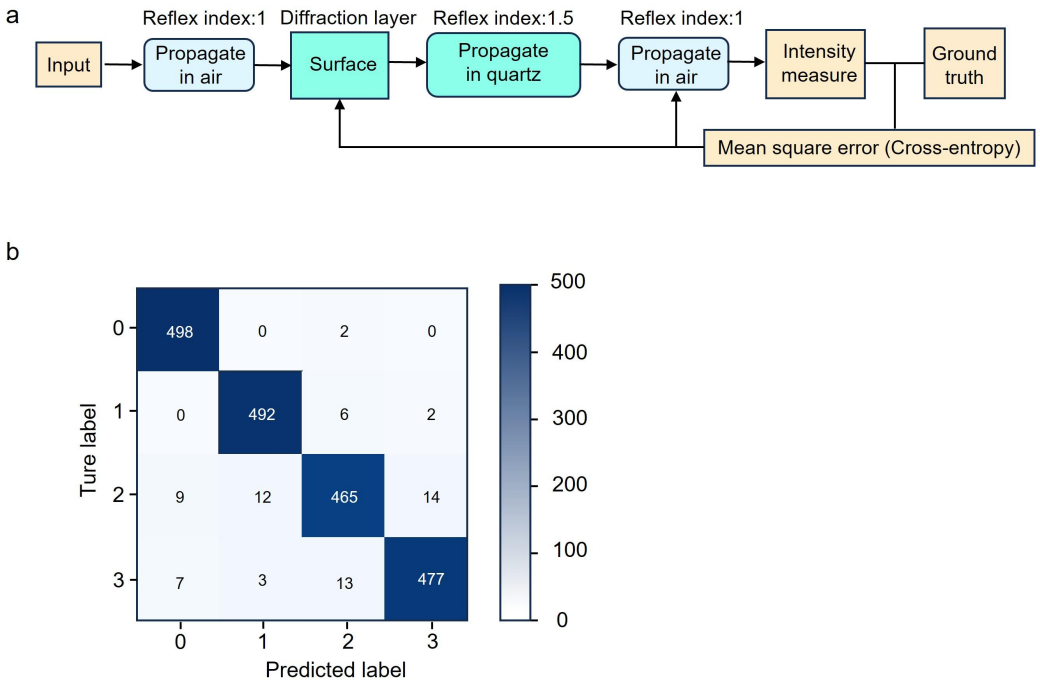

Fig. S13. Training of the diffractive neural network (DNN). a, Schematic diagram of the training process. **b,** Confusion matrix of the simulated classification result.

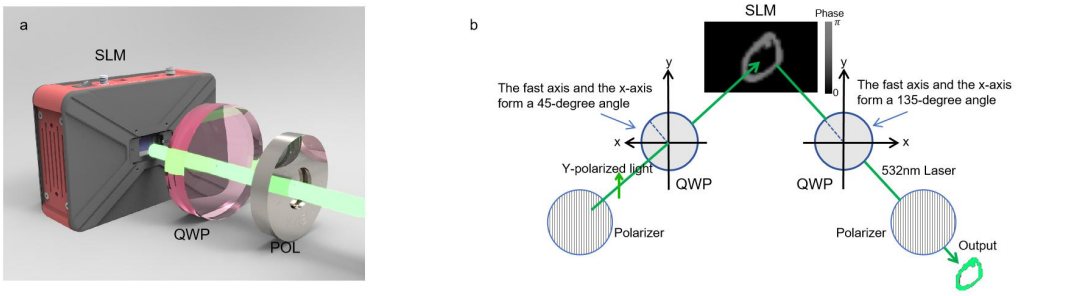

Fig. S14. Amplitude modulation of incident light using the SLM. a, Optical setup. **b**, Schematic illustration of the light propagation process.

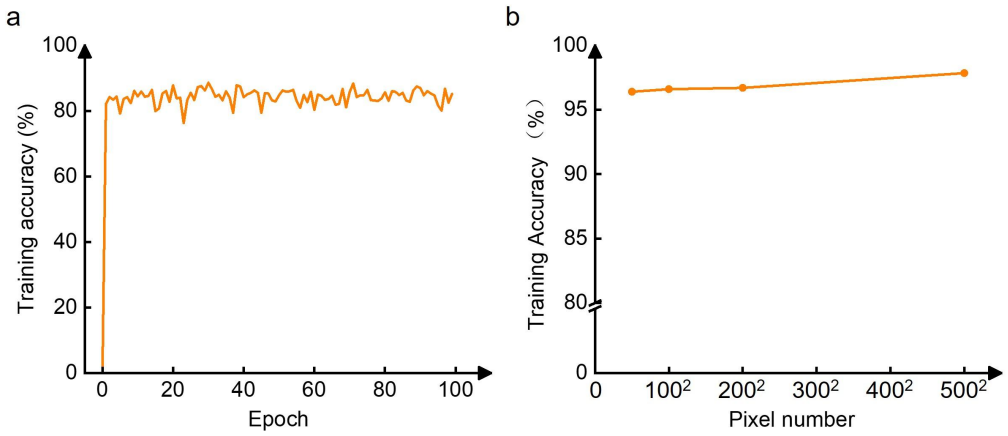

Fig. S15. Performance of single-layer DNNs. a, Training accuracy as a function of training epoch for recognizing 10-class digits. **b,** Training accuracy as a function of the number of pixels in the diffractive layer for recognizing 4-class digits.